Desalination and Water Treatment 320 (2024) 100627

Contents lists available at ScienceDirect

Desalination and Water Treatment

journal homepage: www.sciencedirect.com/journal/desalination-and-water-treatment/

# Biofouling control of thermophilic bacteria in membrane distillation

Lebea N. Nthunya[a,*], Tshepiso J. Mpala[a], Anita Etale[b], Oranso T. Mahlangu[c], Mahloro Hope Serepa-Dlamini[d], Eduardo A. Lopez-Maldonado[e], Heidi Richards[a,*]

[a] Molecular Sciences Institute, School of Chemistry, University of the Witwatersrand, Private Bag X3, Johannesburg 2050, South Africa
[b] Department of Aerospace Engineering, School of Civil, Aerospace, and Mechanical Engineering, University of Bristol, Bristol BS8 1TR, United Kingdom
[c] Institute for Nanotechnology and Water Sustainability, College of Science, Engineering and Technology, University of South Africa, Florida 1709, Johannesburg, South Africa
[d] Department of Biotechnology and Food Technology, University of Johannesburg, Doornfontein Campus, P.O. Box 17011, Johannesburg 2028, South Africa
[e] Faculty of Chemical Sciences and Engineering, Autonomous University of Baja California, 22424 Tijuana, B.C., Mexico

ARTICLE INFO

*Keywords:*
Biofouling
Membrane distillation
Seawater desalination
Silver nanoparticles
Thermophilic *G. stearothermophilus*

ABSTRACT

Previously, fouling of MD membranes was perceived to be minimal due to the operational conditions preventing bacterial growth. However, recent studies presented fouling of MD membranes, largely due to various halophilic and thermophilic bacterial. The current study presented potential of antibacterial cellulose nanocrystals (CNCs) capped silver nanoparticles (AgNPs) towards biofouling control in MD water desalination processes. Interestingly, the CNCs were used as capping and reducing agent in a microwave mediated synthesis of AgNPs. The green synthesis approach of AgNPs and its successful use in MD processes was reported for the first. The MD experiments were carried out using a series of modified PVDF membranes and feed solution spiked with a thermophilic *G. stearothermophilus*. Upon evaluation of fouled membranes, particularly PVDF, PVP-equipped PVDF, and f-CNTs-modified PVDF, the surface energy of interactions were $-131$ mJ/m$^2$, $-31.5$ mJ/m$^2$, $-28.6$ mJ/m$^2$, suggesting favorable interaction between the membranes and bacterial foulant. The findings of this study were supported by fouling layer and bacterial growth as seen from scanning electron microscopy, atomic force microscopy and Fourier transform infrared results. Upon membrane surface modification using CNCs-capped AgNPs, bacterial growth on membrane surface was reduced. Specifically, the positive cohesion energy between the CNCs-capped AgNPs-modified PVDF membrane and thermophilic bacterial foulant was + 63.2 mJ/m2, distinctly proving reduced fouling. The findings were supported by 5.5 % flux decay of the modified membrane compared to 79.3 % flux decay of virgin PVDF membrane. This suggested a long-term membrane integrity in thermophilic bacterial contaminated feed solutions during the MD water desalination.

## 1. Introduction

Social development largely depends on the availability of natural resources including fresh water [1]. The limitations imposed by freshwater scarcity on humanity remain a common challenge. Desalination is a globally employed process harnessed to alleviate current water shortages through recovery of fresh water from saline, brackish and seawater [2]. Due to changing climate conditions worsening global water shortage, the need to augment fresh water supply is crucial [3,4]. Membrane distillation (MD) emerged as a desalination process capable of treating high saline and mineralised wastewater [5–7]. The process is driven by vapour gradient across membrane interfaces. For this reason, microporous hydrophobic membranes are used to reject non-volatile solutes. The transmembrane passage of volatile substances is induced by a partial vapour pressure, caused by temperature differences across membrane interfaces [8,9]. The rate of water recovery depends on various factors including membrane properties, hydrodynamic conditions, and feed solution composition [10].

Polyvinylidene-fluoride (PVDF) is a hydrophobic polymeric membrane predominantly used in MD. The hydrophobicity of PVDF is desired as it facilitates minimal membrane wetting [11]. Unique to MD, irreversible wetting has been reported to cause a rise in costs through increasing membrane replacements [12,13]. Although highly attractive, PVDF is prone to fouling. While various types of fouling affecting MD membrane process were reported, biofouling was rarely evaluated due to perceived saline feed chemical composition and high temperature harnessing microbial growth [14]. However, thermophilic and halophilic microbes thrive in harsh MD operation conditions, causing

* Corresponding authors.
*E-mail addresses:* nthunyalebea@gmail.com (L.N. Nthunya), heidi.richards@wits.ac.za (H. Richards).

https://doi.org/10.1016/j.dwt.2024.100627
Received 14 May 2024; Received in revised form 10 July 2024; Accepted 20 July 2024

membrane biofouling. Particularly, biofouling refers to the deposition of microbial organisms on the membrane surface, leading to the development of a biofilm [15,16]. Due to the intricacies associated with biological activity, microbial accumulation has become somewhat uncontrollable [17].

During treatment of feed solutions contaminated by microbial foulants, biofouling prevention is crucial. Strategies used to prevent biofouling include pretreatment of the feed solution, membrane modification and membrane cleaning [18,19]. To ensure effective process performance, membranes are modified with metal nanoparticles (MNPs) to impart anti-bacterial properties. The NPs inhibit the bacterial growth through destruction of bacterial cell membrane, thus preventing biofilm development [20]. Due to their high antibacterial activities, cellulose nanocrystals capped silver nanoparticles (CNCs-AgNPs) were incorporated on PVDF membranes to prevent bacterial growth. Bacterial growth inhibition experiments were reported elsewhere [21]. The current study evaluates biofouling control of AgNPs-CNCs-modified PVDF membranes during MD treatment of artificial seawater spiked with a monoculture of thermophilic *G. stearothermophilus*. The current study was motivated by the increased development and successions of biofilm formation despite the harsh MD operating conditions believed to harness growth of bacteria. Similarly, the impact of thermophilic bacteria on MD process performance during water desalination is rarely reported and therefore requires extensive research. Hence, the current study opens a new research direction providing detailed significance of CNCs-capped AgNPs incorporated on PVDF membranes towards biofouling control of thermophilic bacteria in MD systems. The CNCs are desirable as they poses minimal detriment to the environment [22]. Various processes presenting nucleation of AgNPs on CNCs have been extensively investigated and reported in literature. These include one-pot PVP assisted deposition of AgNPs on CNCs [23], in situ deposition of AgNPs into CNC photonic films [24] and direct nucleation of AgNPs on CNCs suspension [25]. These synthetic routes utilized environmentally concerning chemicals including ammonia which are often toxic. Exploitation of greener routes utilizing bio-based substrates such as CNCs as both reducing and capping agents under assisted conditions is imperative. This remains a key requirement for safe water treatment process. For this reason, a greener approach involving microwave mediated synthesis of AgNPs where CNCs were exploited as reducing and capping agent for use in MD fouling control was evaluated. To enable the reduction process, the mixture of $AgNO_3$ and CNCs was irradiated under the microwave, facilitating reduction of the $Ag^+$ ions to AgNPs while the CNCs were oxidized to gluconic acid [21]. Produced AgNPs-capped CNCs were embedded in PVDF membranes for biofouling control of thermophilic bacteria in MD. The findings were reported for the first time, thus providing a suitable one-step solution towards control of membrane biofouling in MD induced by thermophilic bacteria. To improve the mechanical properties, carbon nanotubes enriched with carboxylic functional groups were incorporated into PVDF membranes. The CNTs are excellent materials possessing high thermal stability and mechanical strength, thus making them suitable for MD applications [26].

## 2. Methods and material

### 2.1. Materials

Polyvinylidene-fluoride (PVDF, MW = 534,000 g/mol), polyvinylpyrrolidone (PVP, MW = 360,000 g/mol), sodium chloride (NaCl, ACS reagent, 99.0 %), silver chloride (AgCl, reagentPlus®, 99.0 %), magnesium chloride ($MgCl_2$, anhydrous, 98.0 %), sodium sulphate ($NaSO_4$, anhydrous, 98.0 %), calcium chloride ($CaCl_2$, anhydrous 97.0 %) and potassium chloride (KCl, ACS reagent, 99.0 %), 1 H, 1 H, 2 H, 2 H-perfluoro-octyltriethoxysilane (POTS, ACS reagent, 98 %), toluene (ACS reagent, 99 %), and nitric acid ($HNO_3$, ACS reagent, 99 %) were procured from Sigma Aldrich (United States of America). The CNCs were procured from Nanografi Nano Technology and CNTs from SabiNano (Pty) Ltd (South Africa). The thermophilic strain of bacteria (*G. Stearothermophilus, ATCC no: 12980*) and the 0.5 McFarland standard were purchased from Davies Diagnostics (Pty) Ltd (South Africa). Glutaraldehyde (liquid) was procured from Promark Chemicals (South Africa). Mueller Hinton broth (MHB) and Mueller Hinton agar (MHA) were purchased from Sisco Research Laboratories (Pvt) Ltd (India).

### 2.2. Methods

#### 2.2.1. Preparation of fluorosilanized carbon nanotubes

Fluorosilanized CNTs, termed *f*-CNTs were synthesized following a modified approach [27]. Briefly, 80 ml $HNO_3$ was mixed with 0.5 g CNTs under sonication for 4 h at room temperature, followed by a temperature increase to 60 ºC for 24 h. This was done to allow formation of carboxyl groups on the surface of CNTs for further modification. Following acidification, CNTs were centrifuged at 4000 revolutions per minute (rpm) for 20 min and rinsed with DI water to ensure complete removal of residual acid. The CNTs were later dried at 60 ºC overnight. Fluorosilanization of modified CNTs (Fig. 1) involved the dissolution of 0.5 g acidified CNTs in toluene under sonication for 2 h. Then, 20 ml of 0.5 wt% of the POTS toluene solution (prepared by dissolving 0.5 g of POTS in 100 ml toluene) was added into the CNTs mixture and the resultant solution was stirred for 24 h. Produced (*f*-CNTs herein) were washed with toluene and dried at 60 ºC overnight.

#### 2.2.2. Preparation of cellulose nanocrystals-capped silver nanoparticles

Preparation of CNC-capped AgNPs was carried out following a method reported elsewhere [21]. Briefly, 50 ml of AgNO3 (0.1 M) was added into a flask containing 100 ml of CNCs (1 mg/ml). To adjust the pH of the CNCs and $AgNO_3$ to 10, NaOH (0.1 M) was added to the flask drop wisely. The resultant mixture was placed in a microwave reactor and the reaction was carried out at following operating conditions; power settings, stirring speed, and temperature of 500 W, 600 rpm, and 60 ∘C, respectively. Resultantly, the $Ag^+$ ions were reduced to AgNPs while CNCs were oxidized to gluconic acid. The CNCs-capped AgNPs were separated from the mixture and dried at 60 ˚C.

#### 2.2.3. Preparation of PVDF membranes

A solution containing 15 % (w/v) PVDF was prepared using a mixed solvent system of DMAc/DMF (3:2) and various non-solvent additives

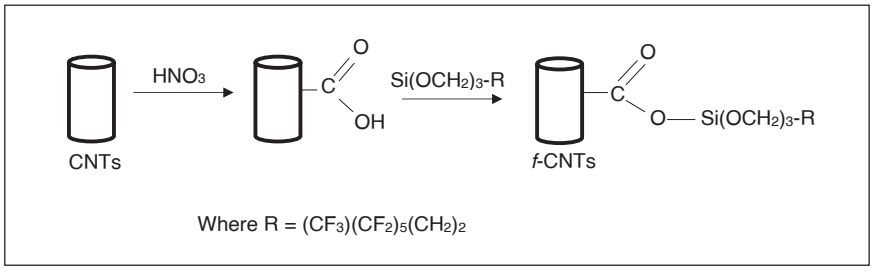


**Fig. 1.** Interaction between CNTs and POTS to produce *f*-CNTs.

**Table 1**
Casting solution composition for each membrane.

| Membrane | PVDF (wt%) | PVP (wt%) | *f*-CNTs (wt%) | CNC-AgNP (wt%) | DMF (wt%) | DMAc (wt%) |
|---|---|---|---|---|---|---|
| A | 15.0 | - | - | - | 51.0 | 34.0 |
| B | 15.0 | 0.1 | - | - | 50.9 | 34.0 |
| C | 15.0 | 0.1 | 0.5 | - | 50.6 | 33.8 |
| D | 15.0 | 0.1 | 0.5 | 6 | 47.0 | 31.4 |

according to the requirements of each membrane (Table 1). The DMAc/DMF increases solvent diffusion rate during coagulation, thus forming large magnitude of small sized figure like pore structures, giving rise to small pore sizes and high porosity [28]. The choice of this mixed solvent system was motivated by the key required properties of MD membranes, namely small pore sizes (0.1–0.4 μm) and high porosity (> 70 %) [29,30]. The polymer solution containing the reagents was stirred until full dissolution and degassed. The solution was cast on a glass plate using a casting knife film applicator with the height set at 80 μm. The wet films were immersed in a tap water bath at room temperature and coagulated, followed by air-drying for 48 h. To improve the antibacterial activity of the membranes, 6 wt% CNC-capped AgNPs was coated on the surface of the membrane during casting. To do so, 6 wt% CNC-capped AgNPs was added in a casting solution of PVDF and mixed. After degassing, the solution was cast on adjusted height 90 μm of the casting knife to ensure the appropriate stability of the antibacterial surface coat. Technically, the PVDF without NPs was casted simultaneously with the coating layer, though at lower height (80 μm) of the casting knife while the coating layer enriched with CNC-capped AgNPs at adjusted higher height (10 μm above 80 μm giving rise to a total height 90 μm. This was done to ensure polymer compatibility and stability of the coating layer. The 6 wt% coating of the CNC-capped AgNPs was chosen based on optimization procedure of the minimum inhibitory concentration (MIC) of CNCs-capped AgNPs reported elsewhere [21]. According to MIC of AgNP and cell viability tests against various strains of bacteria, 6 wt% CNC-capped AgNPs presented 98 % cell reduction or bacterial growth inhibition.

### 2.2.4. Feed solution composition

The synthetic seawater feed solution was composed of 24.5 g/L NaCl, 5.2 g/L $MgCl_2$, 4.1 g/L $NaSO_4$, 1.1 g/L $CaCl_2$, and 0.69 g/L KCl. The feed solutions were prepared from distilled water (conductivity ~ 0.691 μS/cm). Prior to MD experiments, the feed solution was spiked with *G. Stearothermophilus* ($10.0 \times 10^7$ CFU·ml$^{-1}$). Notably, *G. Stearothermophilus* is a Gram-positive, rod-shaped bacterium capable of surviving high temperatures (55ºC – 65 ºC) [31]. To prepare *G. Stearothermophilus* solution, the vial containing bacteria was equilibrated to room temperature (from 4 ºC). Afterwards, one LYFO DISK of *G. Stearothermophilus* was removed aseptically from the vial and placed in sterile water (0.5 ml). The disk was crushed with a sterile swab until the suspension became homogenous. Immediately, the swab was heavily saturated with the suspension and transferred to an MHA medium. The swab was rolled one-third of the plate and streaked to isolate colonies using a sterile loop. Lastly, the agar plate was incubated at 60 ºC for 24 h. Further bacterial strain growth was conducted in MHB where 0.5 McFarland standard was used to obtain the optimal density of the cultured bacteria. Detailed preparation of bacterial culture was reported elsewhere [21].

### 2.2.5. Evaluation of direct contact membrane distillation performance

Laboratory scale direct contact membrane distillation (DCMD) experiments were conducted to evaluate membrane performance (Fig. 2). The active surface of the membranes was 1.147 m$^2$. The plate and frame membrane module were used during a 24 h MD tests. The solutions were circulated in a counter-current direction at a crossflow velocity of 412 ml·min$^{-1}$ using a peristaltic pump (Cole Parmer Ltd, Masterflex). The feed and permeate solution temperatures were maintained at 60 ºC and 15 ºC, respectively. Salt rejection and permeate flux (calculated using Eqs. (1) & (2)) were evaluated by monitoring and recording the change in distillate conductivity and weight respectively.

$$R\% = \frac{k_f - k_p}{k_f} * 100\% \quad (1)$$

$$J = \frac{m}{A*t} \quad (2)$$

*Where R%, $k_f$, $k_p$, J, m, A* and *t* represents the salt rejection (%), feed conductivity (μS·cm$^{-1}$), permeate conductivity (μS·cm$^{-1}$), permeate flux (kg·m$^{-2}$·h$^{-1}$), the mass obtained from the weighing balance (kg), the effective membrane area (m$^2$) and time (h) respectively.

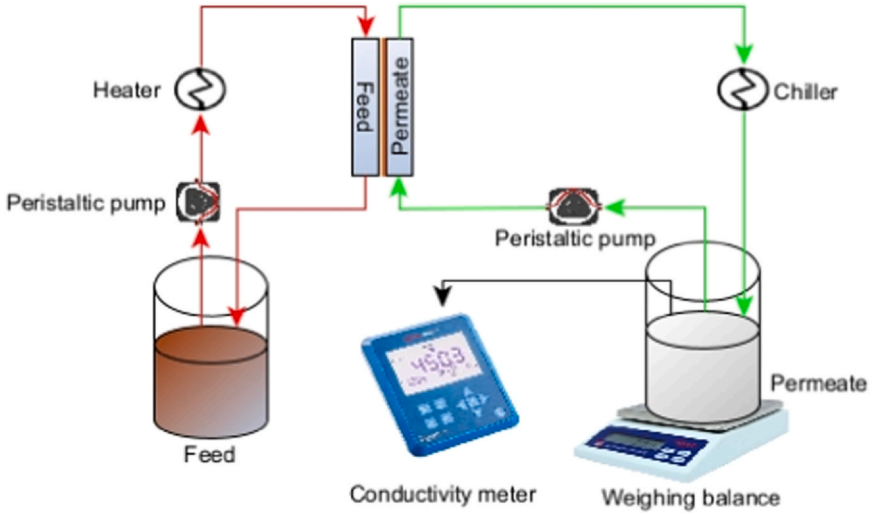


**Fig. 2.** Counter current flow direct contact membrane distillation for water desalination in the presence of thermophilic bacteria [32].

**Table 2**
The surface tension properties of the probe liquids at 20 °C [37].

| Probe liquids | $\sigma_L^D$ (mJ·m$^{-2}$) | $\sigma_L^+$ (mJ·m$^{-2}$) | $\sigma_L^-$ (mJ·m$^{-2}$) | $\sigma_L^P$ (mJ·m$^{-2}$) | $\sigma_L^{TOT}$ (mJ·m$^{-2}$) |
|---|---|---|---|---|---|
| Water | 21.8 | 25.5 | 25.5 | 51.0 | 72.8 |
| Glycerol | 34.0 | 3.9 | 57.4 | 30.0 | 64.0 |
| Diiodomethane | 50.8 | 0.0 | 0.0 | 0.0 | 50.8 |

*2.2.6. Characteristic analysis of the membranes*

Membrane fouling was evaluated using various direct and indirect techniques. Briefly, membrane was removed from the module after MD experiments, rinsed with sterilized water, treated with 2.5 % glutaraldehyde to facilitate the immobilization of bacteria, and stored at 4 ºC in the fridge for analysis. To evaluate the membrane-foulant interaction, an indirect contact angle approach was used. Currently, this approach is the most utilized to evaluate solid materials interaction due to lack of direct methods. Three probe liquids namely; deionized water, glycerol and diiodomethane with known surface tension components (Table 2) were used for contact angle measurements using the Kruss Drop Shape Analyzer, DSA30 (KRUSS GmbH, Germany). The contact angles (14 measurements) were recorded using a sessile drop method where 3 µL of the liquids was dropped on the membrane surface. Through modelling processes, the surface energy of the solid was expressed as the sum of the dispersive Liftshitz-van der Waals ($\sigma^D$) and polar ($\sigma^P$) components of surface free energy (Eqs. (3) & (4)). The detailed model of the membrane-foulant interactions were reviewed and reported elsewhere [33]. Other studies analyzed the membrane-foulant interaction through evaluation of cohesive forces as estimated by these models [34–36]. The Young-Dupre model was used to derive the surface free energy of the fouled membranes from the contact angles of three probe liquids (Eq. (5)). The interfacial free energy between the membrane ($m$) and foulant ($s$) in water ($l$) was estimated using Eqs. (6)–(8).

$$\sigma^{TOT} = \sigma^D + \sigma^P \tag{3}$$

$$\sigma^P = \sqrt{\sigma^+\sigma^-} \tag{4}$$

$$\sigma(1 + \cos\theta) = 2\sqrt{\sigma_s^D\sigma_s^D} + \sqrt{\sigma_s^+\sigma_l^-} + \sqrt{\sigma_s^-\sigma_l^+} \tag{5}$$

$$\Delta G_{swm}^D = 2(\sqrt{\sigma_l^D} - \sqrt{\sigma_s^D})(\sqrt{\sigma_m^D} - \sqrt{\sigma_l^D}) \tag{6}$$

$$\Delta G_{swm}^P = 2\sqrt{\sigma_l^+}(\sqrt{\sigma_s^-} + \sqrt{\sigma_m^-} - \sqrt{\sigma_l^-}) + 2\sqrt{\sigma_l^-}(\sqrt{\sigma_s^+} + \sqrt{\sigma_m^+} - \sqrt{\sigma_l^+}) - 2\sqrt{\sigma_s^+\sigma_m^-} - 2\sqrt{\sigma_s^-\sigma_m^+} \tag{7}$$

$$\Delta G_{swm}^{TOT} = \Delta G_{swm}^D + \Delta G_{swm}^P \tag{8}$$

Where $\sigma^{TOT}$ is the total surface tension, $\sigma^D$ and $\sigma^P$ are the dispersive and polar components, $\sigma^-$ and $\sigma^+$ are the electron donor and electron acceptor of the polar component, $\theta$ is the measured contact angle, $s$ and $l$ are the solid and liquid phases respectively, $\Delta G_{swm}^{TOT}$ is the total free energy of cohesion.

The fouling layer of the membrane was assessed using TESCAN Vega scanning electron microscope (SEM). Prior to SEM analysis, all samples were sputter coated using gold/palladium (Au/Pd) to minimize sample charging. The atomic force microscopy (AFM, Witec Alpha 300 A, TS-150) analysis was conducted at a scanning area of 2.0 µm × 2.0 µm. This was done to evaluate the roughness of the fouled membranes. To evaluate the chemical interaction between bacterial foulant and the membranes, the Fourier transform infrared analysis was carried out at a scanning range of 500 cm$^{-1}$ to 4000 cm$^{-1}$ using Tensor 27 FTIR, Bruker, South Africa (PTY) LTD). Similarly, the FTIR was used to understand the chemical formation of CNCs-capped AgNPs under the similar conditions as membranes. Other characteristic analysis of the CNCs-capped AgNPs were carried out using various techniques including Bruker D2 X-ray diffraction, PerkinElmer UV-Vis spectrometer, FEI Tecnai T12 TEM coupled with energy dispersive spectroscopy (EDS) and the findings were reported elsewhere [21].

## 3. Results and discussion

### 3.1. FTIR analysis of cellulose nanocrystals-capped silver nanoparticles

The FTIR spectra of CNCs and CNC-capped AgNPs is illustrated in Fig. 3a. For CNCs, the broad peak at 3328 cm$^{-1}$ was attributed to the symmetric and asymmetric stretching of the OH functional groups on the surface of CNCs [38]. The band position of the C-O-C peak at 1014 cm$^{-1}$ demonstrated a significantly strong intensity of adsorption, forming part of the bulk material of cellulose [39]. The peaks at 2906 cm$^{-1}$ and 1315 cm$^{-1}$ were attributed to the stretching C-H alkyl peak and the bending C-H peak, respectively. There was a significant decline in intensity of the OH peak (as well as a shift toward a lower wavenumber) for the CNC-capped AgNPs, potentially due to the interaction of AgNPs with the OH groups. Similar results were reported elsewhere [22], although their shift in position of the OH peak was towards a higher wavenumber. These alterations in spectra imply the significant role that OH groups play in forming and stabilizing AgNPs [40]. Also, there was a slight shift in the C-O-C band position from 1014 cm$^{-1}$ to 990 cm$^{-1}$, denoting the physical deposition of AgNPs [41]. The appearance of the absorption band at 1240 cm$^{-1}$ demonstrated the formation of an ester group, a product of cellulose decarboxylation. The FTIR analysis was further conducted to analyze various functional groups of CNTc and f-CNTs (Fig. 3b). Absorption peaks occurring at 1486 cm$^{-1}$, 1585 cm$^{-1}$, 2099 cm$^{-1}$ and 2334 cm$^{-1}$ were attributed to C-H, C═C, COOH, and C-O stretching bands, respectively. A shift in FTIR spectra (red shift) was observed upon CNTs reaction with POTS, a

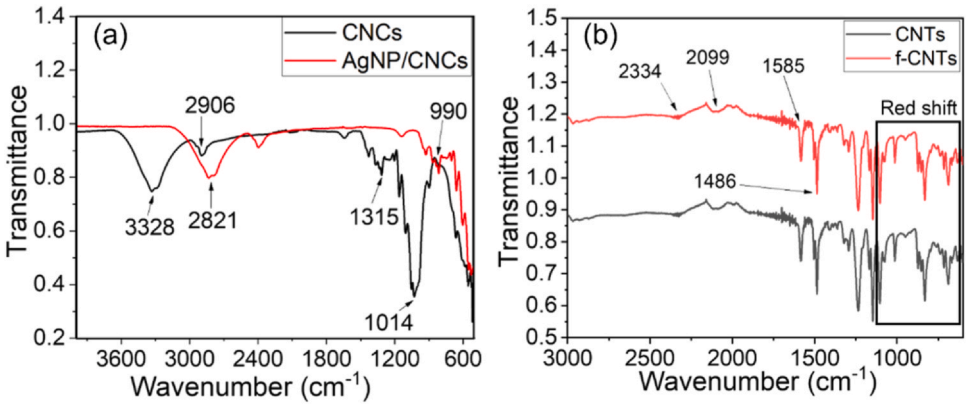


**Fig. 3.** FTIR spectra of (a) CNCs and CNC-capped AgNPs and (b) CNTs and f-CNTs.

**Table 3**
Surface energy components of fouled membranes.

| Membranes | Membrane water contact angle (°) | Surface tension components | | | | | |
|---|---|---|---|---|---|---|---|
| | | $\sigma_s^-$ (mJ/m$^2$) | $\sigma_s^+$ (mJ/m$^2$) | $\sigma_s^P$ (mJ/m$^2$) | $\sigma_s^D$ (mJ/m$^2$) | $\sigma_s^{TOT}$ (mJ/m$^2$) | ΔG (mJ/m$^2$) |
| A | 60.49 | 14.6 | 18.3 | 30.8 | 1.17 | 31.9 | −131 |
| B | 77.02 | 4.01 | 6.95 | 10.6 | 11.4 | 22.0 | −31.5 |
| C | 88.41 | 2.47 | 20.1 | 14.1 | 45.9 | 60.0 | −28.6 |
| D | 83.07 | 161 | 21.2 | 117 | 17.7 | 135 | + 63.2 |

(a) PVDF membrane, (b) PVDF membrane equipped with pore-forming PVP, (c) f-CNTs-modified PVDF membrane, (d), f-CNTs/CNC-AgNPs-modified PVDF membrane

phenomenon depicting chemical structural changes occurring during Fluorosilanization.

### 3.2. Membrane-foulant interactions

Synergistic interactions between membranes and thermophilic bacteria were evaluated through sequential modeling of pristine and fouled membranes. This was achieved through correlation of dispersive and polar energy interactions. The surface interaction energy was estimated through an indirect contact angle approach where van Oss and Young-Dupre models were used. Similar detailed methods were reviewed and reported elsewhere [33]. Based on contact angle measurements, the liquid forms three interfaces, namely, solid-liquid, solid-gas and liquid-gas upon interacting with the surface of virgin or fouled membrane. These surface tensions of the solid and liquid phase determine the formation of the contact angle. Through these contact angle measurements, the surface tension components were used to describe the forces between the membrane and microbial foulants. Liftshitz-van der Waals components of the liquid phase were larger for all membranes compared to the solid phase (i.e. $\sigma_l^D > \sigma_s^D$) suggesting repulsive interactions [36]. Based on large dispersive component values, particularly f-CNTs-modified PVDF membrane (Table 3), the interactions between membranes and microbial foulant were caused by London dispersion force induced by membrane surface and foulant in proximity. Upon approaching each other, the electron cloud between the membrane and bacterial foulant creates weak repulsion forces. However, non-dispersive forces hydrogen, dipole-dipole, apolar, polar and hydrophobic interactions influence the membrane and foulant interaction. Based on interaction cohesion forces (Table 3), the interaction of foulant and all membranes was highly favorable. Forces of cohesion were $-131$ mJ/m$^2$, $-31.5$ mJ/m$^2$, $-28.6$ mJ/m$^2$ for PVDF, PVP-equipped PVDF, and f-CNTs-modified PVDF membranes suggesting a decrease in membrane-foulant interaction upon membrane modification. Despite modification of f-CNTs-modified PVDF membranes, membrane-foulant interaction remained cohesively attractive. Incorporation of CNCs-AgNPs on the membrane surface lessened the biofoulant deposition through reduced interaction as evidence by a positive value (+ 63.2 mJ/m$^2$) of cohesion attraction forces (Table 3). Similarly, the high electron donor component of f-CNTs/CNCs-AgNPs-modified PVDF membranes justified repulsive short-range acid-base interaction between the f-CNTs/CNCs-AgNPs-modified PVDF membrane and the *G. Stearothermophilus* [42].

### 3.3. DCMD performance evaluation using saline water spiked with bacteria

Impact of biofouling on DCMD process performance was evaluated in a 24 h laboratory experiment (Fig. 4). Herein, synthetic seawater spiked with a monoculture of *G. Stearothermophilus* was used as the feed solution. The water flux of PVDF membrane decreased considerably as a function of time, with a final decline of 79.3 %. This was a substantial flux decay compared to the flux decline (6.5 %) in the absence of biofoulant as per previous reported findings [32]. 79.3 % decline obtained herein was attributed to the development of a biofouling layer on the membrane surface (Fig. 4). Technically, the biofouling layer (biofilm formation) on the membrane surface increased mass transfer resistance of the water vapour molecules, reducing the rate of water recovery (permeate flux) [12,33]. Rapid bacterial growth on pristine PVDF and bacterial growth inhibition on the surface of f-CNTs/CNC-AgNPs-modified PVDF membrane were reported elsewhere [21]. The rapid bacterial growth was motivated by the presence of high number of live cells as per viability tests. However, 98 % of live cells were reduced on the surface of the f-CNTs/CNC-AgNPs-modified PVDF membrane, Indicating the capacity of AgNPs to inhibit bacterial growth on the membranes [21]. During DCMD experiments, bacterial adhesion on the membrane surface secreted extracellular polymeric substance (EPS), thus maintaining the upkeep of the stagnant fouling layer. Adhesion of bacteria is caused by many factors, including hydrodynamic conditions, feed solution composition, physiochemical properties of the bacteria and membrane properties [10,43]. In this study, 60 ºC inspired optimal growth temperature of *G. Stearothermophilus*, thus promoting large population interaction with the membrane, resulting in a consequential deposition of bacterial cells [31]. In a similar study, Bogler & Bar-Zeev, [44] assessed the impact of *Anoxybacillus sp*. on MD performance under different feed solution temperatures [44]. The study reported 78 % water flux decline at 55 ºC, largely attributed to the favored growth of *Anoxybacillus sp.* Evidently, parameters optimization of MD operation is imperative, mainly because different feed solution compositions affect the process performance differently. Once adhered, these fouling layers induce mass and heat transfer resistance, causing a decrease in process driving force [45]. Consequently, the water flux and salt rejection decreases. This is evidenced by an increase in process conductivity of PVDF membrane, where the distillate conductivity increased to 82 µS/cm. Though the conductivity increased steadily, salt rejection remained satisfactory (~ 99.8 %). Therefore, impact of bacterial inoculation on salt rejection was minimal.

The process water flux of PVP-equipped PVDF and f-CNTs-modified PVDF membranes fluctuated considerably as a function of time, albeit with minimal variation. The findings presented 17.7 % and 15.8 % decay flux for PVP-equipped PVDF and f-CNTs-modified PVDF membranes respectively from the initial to the final experimental test time. Similarly, membrane fouling decreased salt rejection of PVP-equipped PVDF and f-CNTs-modified PVDF membranes as evidenced by increased permeate conductivity from approx. 5 µS/cm to 188.9 µS/cm and 160.0 µS·cm$^{-1}$ respectively, possibly due to wetting of the membrane. Similar findings were reported by Elcik et al., (2022) where permeate conductivity increased to 140 µS·cm$^{-1}$ at 65 ºC. The water contact angles of fouled membranes decreased to 60.5º (PVDF membrane), 77.0º (PVP-equipped PVDF) and 88.4º (f-CNTs-modified PVDF membranes) suggesting membrane wetting. Based on Teoh et al. (2021) reported findings, the increase in permeate conductivity beyond 20 µS·cm$^{-1}$ present possible occurrence of membrane wetting. These findings were supported by Ahn et al. (2021) despite high salt rejection (99 %) of the wetted PVDF membranes. For these reasons, the biofouling *G. Stearothermophilus* influenced wetting of all membranes tested in the current study, thus increasing the distillate conductivity considerably. Although membrane pores should retain resistance to wetting for

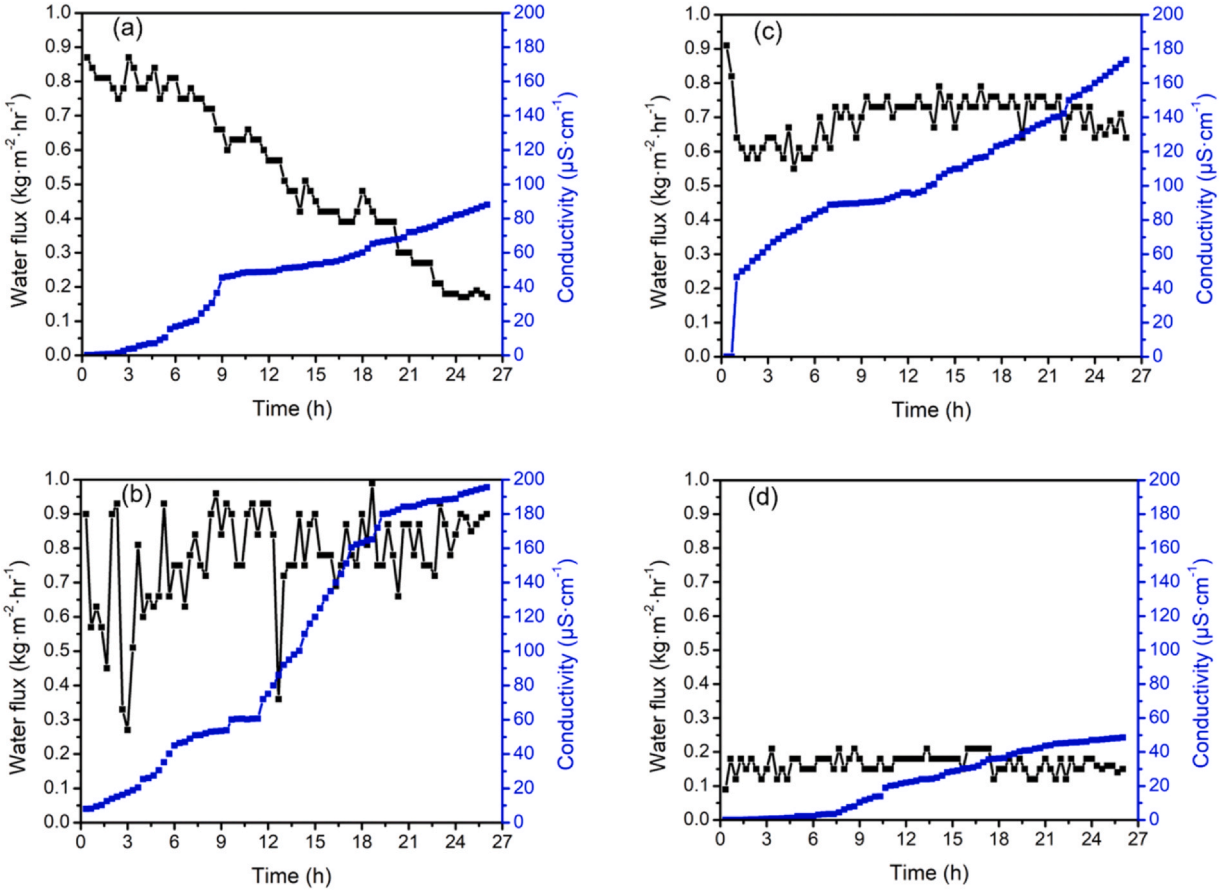


**Fig. 4.** Water flux and distillate conductivity in DCMD water desalination where synthetic seawater spiked with thermophilic bacteria used as feed solution: (a) PVDF membrane, (b) PVDF membrane equipped with pore-forming PVP, (c) f-CNTs-modified PVDF membrane, (d), f-CNTs/CNC-AgNPs-modified PVDF membrane.

effective MD process, the wetting of these membranes is inevitable, thus degrading process efficacy [46]. Therefore, fouling mitigation minimizing membrane wetting is imperative.

The process water flux of f-CNTs/CNC-AgNPs-modified PVDF membrane remained relatively stable as a function of time, averaging to 0.165 $kg{\cdot}m^{-2}{\cdot}hr^{-1}$. The flux declined by 5.5 % during a 26-h experiment test. Distillate conductivity remained relatively low with minimal increase to 47 $\mu S{\cdot}cm^{-1}$. Trivial increase in distillate conductivity presented membrane resistance to wetting. Process performance stability was attributed to the presence CNC-capped AgNPs capable of inhibiting bacterial growth on membrane surface (Fig. 4**&** 5). Bacterial growth resistance of f-CNTs/CNC-capped AgNPs-modified PVDF membrane was reported elsewhere [21]. Due to application of the modified membranes in water treatment, determination of AgNPs leach is imperative [47,48]. Our previous study ascertained sustainable attachment of the AgNPs on PVDF membrane with minimal leaching [32]. Compared to other studies, the current findings presented a remarkable resistance to flux decay due to incorporation of the antibacterial AgNPs on the surface of the PVDF membrane (Table 4**)**. This study demonstrates the potential application of f-CNTs/CNC-capped AgNPs towards minimization of fouling in MD systems.

### *3.4. The SEM analysis of fouled membranes*

The surface morphology of the fouled membranes was evaluated and presented in Fig. 5. The PVDF membrane developed a connected cobweb-like microbial mat, largely covering the feed side of the membrane surface **(**Fig. 5**)**. Similar findings were recorded on PVP-equipped PVDF membrane. The PVP alters physical properties through enhanced pore formation without changing chemical properties. Therefore, improved formation of membrane pores does not provide resistance towards biofilm formation on membrane surface. Remarkably, EPS was released by bacteria, enhancing the inter-connectedness of the fouling layer, consequently lowering the rate of water recovery [53]. A reduced production of water flux was attributed to an increase in the mass and heat transfer resistance induced by a rise in resistance of vapour transport across the membrane. Also, f-CNTs-modified PVDF membranes recorded the connected fouling layer with minimal bacterial growth. Additionally, surface morphology of the membrane changed considerably. To understand the formation of the biofilm layer, the cross-section of the pristine membranes, previously reported [32] and the fouled membranes in the current study were compared. The cross-sectional view of PVDF, PVP-equipped PVDF and f-CNTs-modified PVDF membranes presented the biofilm layer of 6.3 µm, 5.0 µm and 4.4 µm respectively. However, the biofilm layer on f-CNTs/CNC-AgNPs-modified PVDF membrane was indeterminable due to the minimal growth. Notably, the biofilm presented in Fig. 5 is a fractional representation of the membrane surface and not a total representation of the biofilm layer. Bacterial micrographs on PVDF, PVP-equipped PVDF and f-CNTs-modified PVDF membranes presented rod-shaped structures, a confirmation of *G. Stearothermophilus* growth [31]. A significant interaction between cells presented a firmly connected fouling layer (Fig. 5). Similar images were reported by Zheng et al., (2022) during MD treatment of desulfurized wastewater where microbial distribution and succession on the membrane surface was studied. However, CNC-AgNPs modification of the PVDF membranes inhibited growth of bacterial, thus presenting a deposit of a minimized layer with no clear structural morphology of the bacteria.

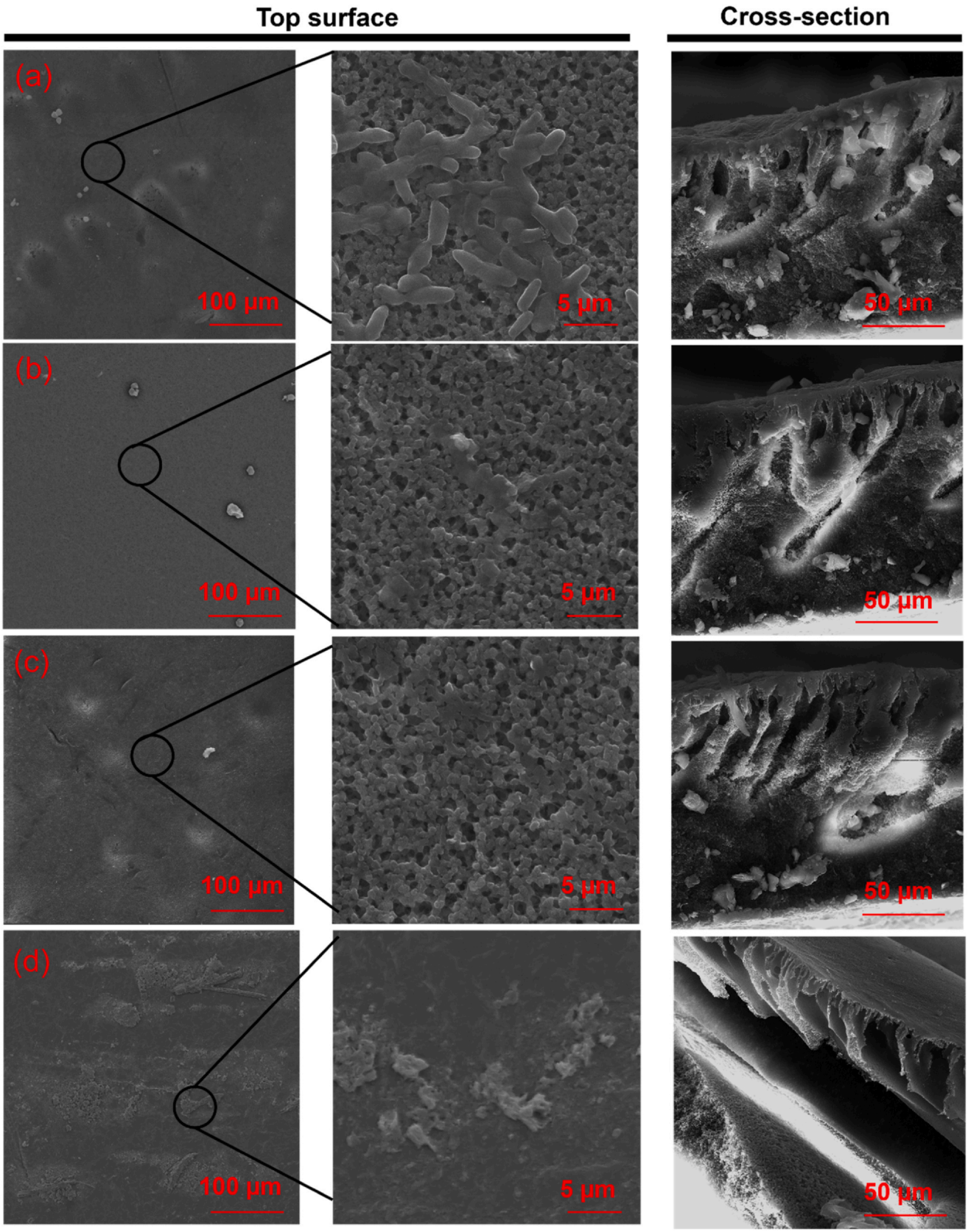


**Fig. 5.** The SEM micrographs of membranes fouled by thermophilic *G. Stearothermophilus* during DCMD seawater desalination; (a) PVDF membrane, (b) PVDF membrane equipped with pore-forming PVP, (c) f-CNTs-modified PVDF membrane, (d), f-CNTs/CNC-AgNPs-modified PVDF membrane.

**Table 4**
Effect of membrane biofouling on flux as a function of time. Comparing the literature with the findings of the current study.

| The MD configuration | Membrane | Foulant and test duration | Findings | Ref. |
|---|---|---|---|---|
| DCMD<br>$T_F$ = 55 °C<br>$T_p$ = 20 °C | PE-supported PTFE | $1.7 \times 10^8$ cells $ml^{-1}$ of mesophilic bacteria from Red Sea, MD operation time = 72 h. | 75 % flux decay (from 32 to 8 $L{\cdot}m^{-2}{\cdot}h^{-1}$) | [49] |
| DCMD<br>$T_F$ = 60 °C<br>$T_p$ = 15 °C | PTFE | $8.9 \times 10^5$ cells of picophytoplankton, MD operation time = 96 h | 50 % flux decay (from normalized flux of 1.0 to 5.1 $L{\cdot}m^{-2}{\cdot}h^{-1}$) | [50] |
| DCMD<br>$T_F$ = 60 °C<br>$T_p$ = 10 °C | PTFE | Lake water from China characterized by a mix of bacterial strains, MD operation time = 360 h. | 55 % flux decay (from normalized flux of 1.0 to 0.45 $L{\cdot}m^{-2}{\cdot}h^{-1}$) | [51] |
| DCMD<br>$T_F$ = 60 °C<br>$T_p$ = 20 °C | AgNP/f-MWCNTs-modified PVDF | Thermophilic bacteria effluent from Innolab (http://www.innolab.be/), Ghent, MD operation time = 50 h. | 47 % flux decay (from 12.8 to 6.7 $L{\cdot}m^{-2}{\cdot}h^{-1}$) | [52] |
| DCMD<br>$T_F$ = 60 °C<br>$T_p$ = 15 °C | f-CNTs/CNC-AgNPs-modified PVDF | Synthestic seawater spiked with 10.0 × 107 CFU.ml − 1 G. Stearothermophilus, MD operation time = 26 h. | 5.5 % flux decay (from 0.18 to 0.17 $L{\cdot}m^{-2}{\cdot}h^{-1}$) | This study |

### 3.5. The AFM analysis of fouled membranes

The fouled membranes were evaluated to understand their surface roughness (Fig. 6). Similarly, PVDF membrane reported high surface roughness designated by average roughness (SA) and root mean square roughness (SQ) of 527 nm and 638 nm respectively. Large surface roughness parameters compared to the previously reported membranes [32] was caused by bacterial attachment on membrane surface, EPS secretion and biofilm development as evidenced by SEM and FTIR results. The SA and SQ of the previously reported PVDF membrane before fouling were 15.9 nm and 21.7 nm respectively [32]. The difference in roughness parameters supports the projected membrane surface modification or formation of the biofilm layer. The surface roughness of PVP-equipped PVDF and f-CNTs-modified membranes were lower compared to PVDF membrane. This was attributed to a low fouling layer as evidenced from the SEM results. Nonetheless, the SA and SQ values increased compared to the previously reported membranes [32] due to the succession and evolution of biofilm development. The AFM peaks and valleys of fouled membranes present a change in surface topology upon fouling. Albeit higher compared to the previously reported membranes, the change in surface roughness of f-CNTs/CNC-AgNPs-modified PVDF membrane in the current study was insignificant compared to PVDF membrane. The minimal change in membrane surface roughness was evidenced by a slight fouling layer recorded on f-CNTs/CNC-AgNPs-modified PVDF membrane (see SEM micrographs on Fig. 5). This was attributed to CNC-capped AgNPs modification of PVDF ensuring bacterial growth resistance. Nonetheless, the SA (132 nm) and SQ (167 nm) values on f-CNTs/CNC-AgNPs-modified PVDF membrane were higher compared to PVP-equipped PVDF and f-CNTs-modified PVDF membranes, suggesting a rougher membrane. This was attributed to a combination of fouling layer and incorporated NPs within the membrane matrix. Though it changes membrane surface topology, the anti-microbial properties of AgNPs is supported by widely reported studies [54–58]. In the current study, bacterial secretion of extracellular polymeric substances (EPS) in response to minimize cell destruction by the AgNPs was supported by the FTIR analysis presented

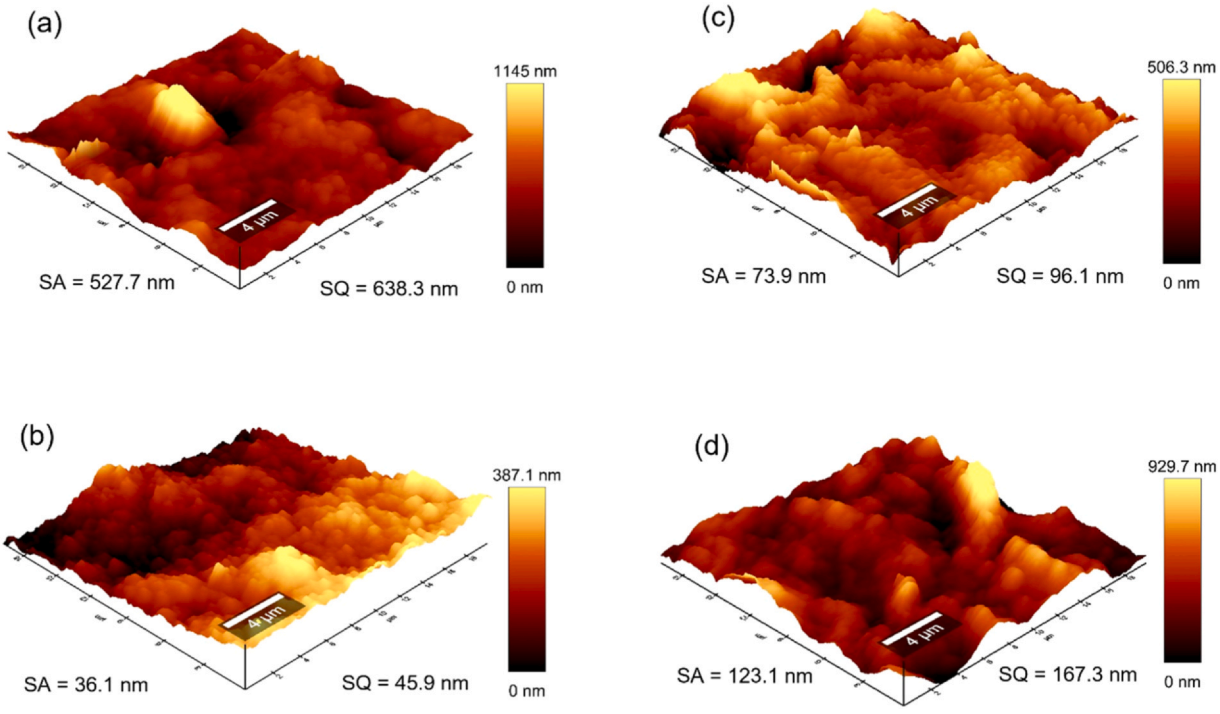


**Fig. 6.** The AFM images of *G. Stearothermophilus*-fouled membranes during DCMD seawater desalination; (a) PVDF membrane, (b) PVDF membrane equipped with pore-forming PVP, (c) f-CNTs-modified PVDF membrane, (d), f-CNTs/CNC-AgNPs-modified PVDF membrane.

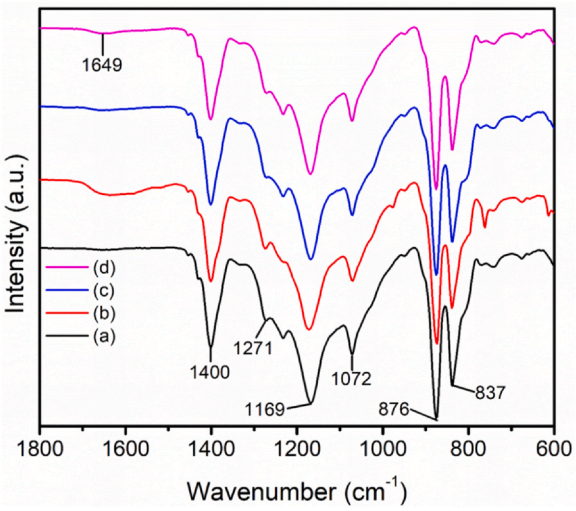


**Fig. 7.** The FTIR spectra of membranes fouled by thermophilic *G. Stearothermophilus* during DCMD seawater desalination; (a) PVDF membrane, (b) PVDF membrane equipped with pore-forming PVP, (c) f-CNTs-modified PVDF membrane, (d), f-CNTs/CNC-AgNPs-modified PVDF membrane.

below. Due to their capability to maintain sustainable antibacterial activity without promoting resistance to growth inhibition, AgNPs are desirable [59]. These NPs ensure prolonged retainment of anti-microbial activity over a sustained period. In summary, these results display the tremendous potential of AgNPs for biofouling mitigation MD water treatment systems. Although considerable interpretations were made from this work, the process of fouling (in MD) is time-dependent, and requires substantial operating time to fully comprehend the impact of membrane characteristics on process performance [60].

### 3.6. The FTIR analysis of fouled membranes

The FTIR analysis of the fouled membranes was carried out to understand their chemical interaction with bacterial foulant (Fig. 7). Due to the absence of peaks at higher frequencies, the reported range was 1800 – 600 $cm^{-1}$. All four membranes exhibited similar peaks with minimal differences. The peaks at 837 $cm^{-1}$ and 876 $cm^{-1}$ correspond to α and β bands of PVDF. These forms of PVDF remained unaltered compared to the previously reported findings of virgin membranes [32]. Other β forms of PVDF shifted to lower absorption frequencies ~1271 $cm^{-1}$ and 1400 $cm^{-1}$ [61]. Similarly, the peak at 1072 $cm^{-1}$ corresponding to the α form of PVDF shifted to higher frequencies [61]. The peak shift was caused by a binding strength between the membranes and bacterial proteins. Technically, the shift was an indication of the overlap of two bands contributed by the PVDF membranes and proteins of *G. Stearothermophilus* [62]. The band at 1169 $cm^{-1}$ was associated with phospholipids, phosphorylated proteins and nucleic acids of the bacterial cells. Also, the broad peak at 1655 $cm^{-1}$ was absorption intrinsic of bacterial amino acids. This band was associated with bacterial secretion of extracellular polymeric substances (EPS) in response to minimization of reduced stress causing bacterial growth inhibition [63]. Upon interaction with AgNPs, the bacteria released the EPS to minimize its cell destruction. Notably, the SEM results presented a tremendous bacterial cell destruction upon interacting with AgNPs.

## 4. Conclusion

The sustainable production of fresh water in MD is restricted by several issues, including biofouling. Since MD operates under moderate to high temperatures, thermophilic strains of bacteria are mostly responsible for biofouling. Herein, CNC/AgNP-modified PVDF membrane was assessed towards biofouling control. The process evaluation was carried out using feed solution spiked with *G. stearothermophilus,* a gram-positive thermophilic strain. Evidently, CNC/AgNP-modified PVDF membrane largely inhibited bacterial deposition and subsequent fouling layer formation, dissimilar to pristine PVDF whose surface was covered with bacteria and a fouling layer. Subsequently, the water flux of virgin PVDF membrane decreased overtime while CNC/AgNP-modified PVDF membrane's water flux remained stable. This was attributed to the minimized bacterial growth induced by AgNPs. Also, 99 % salt rejection remained relatively stable, indicating membrane resistance to wetting. Overall, membrane modification (using AgPs) is a useful tool to minimize biofouling in MD water desalination. Although the current findings suggest a promising solution to address MD membrane biofouling induced by thermophilic bacteria, long-term test experiments are required to ensure the stable performance of CNC-AgNPs-modified PVDF membrane. Similarly, process evaluation using environmental thermophilic bacteria-contaminated salty wastewater is recommended. Despite promising NPs leaching resistant from PVDF membranes, long-term operation will establish the stability of CNC-AgNPs with detailed leaching profiles.

## CRediT authorship contribution statement

Lebea N. Nthunya, Anita Etale, and Heidi Richards contributed to conception and design of the study. Lebea N. Nthunya and Heidi Richards organized the database. Oranso T. Mahlangu, Mahloro Hope Serepa-Dlamini and Eduardo A. Lopez-Maldonad performed membrane characterization and statistical analysis. Tshepiso J. Mpala wrote the first draft of the manuscript. All authors contributed to manuscript revision, read, and approved the submitted version.

## Data availability

Data will be made available on request.

## Declaration of Competing Interest

The authors declare that they have no known competing financial interests or personal relationships that could have appeared to influence the work reported in this paper.

## Acknowledgement

The authors would like to thank the University of the Witwatersrand and National Research Foundation (NRF-grant number: CSRP23042496727) for funding this research work.

## References

[1] Turner K, Naidoo K, Theron J, Broodryk J. Investigation into the cost and operation of southern African desalination and water reuse plants. Water Res Comm 2015;3:1–130.
[2] Cui Z, Li X, Zhang Y, Wang Z, Gugliuzza A, Militano F, Drioli E, Macedonio F. Testing of three different PVDF membranes in membrane assisted-crystallization process: Influence of membrane structural-properties on process performance. Desalination 2018;440:68–77. https://doi.org/10.1016/j.desal.2017.12.038.
[3] Tsai JH, Macedonio F, Drioli E, Giorno L, Chou CY, Hu FC, Li CL, Chuang CJ, Tung KL. Membrane-based zero liquid discharge: Myth or reality? J Taiwan Inst Chem Eng 2017;80:192–202. https://doi.org/10.1016/j.jtice.2017.06.050.
[4] Liu HB, Li B, Guo LW, Pan LM, Zhu HX, Tang ZS, Xing WH, Cai YY, Duan JA, Wang M, Xu SN, Tao XB. Current and Future Use of Membrane Technology in the Traditional Chinese Medicine Industry. Sep Purif Rev 2022;51:484–502. https://doi.org/10.1080/15422119.2021.1995875.
[5] Rajwade K, Barrios AC, Garcia-Segura S, Perreault F. Pore wetting in membrane distillation treatment of municipal wastewater desalination brine and its mitigation by foam fractionation. Chemosphere 2020;257:127214. https://doi.org/10.1016/j.chemosphere.2020.127214.
[6] Mokhtar NM, Lau WJ, Ismail AF, Veerasamy D. Membrane distillation technology for treatment of wastewater from rubber industry in Malaysia. Procedia CIRP 2015;26:792–6. https://doi.org/10.1016/j.procir.2014.07.161.
[7] Guillen-Burrieza E, Ruiz-Aguirre A, Zaragoza G, Arafat HA. Membrane fouling and cleaning in long term plant-scale membrane distillation operations. J Memb Sci 2014;468:360–72. https://doi.org/10.1016/j.memsci.2014.05.064.

[8] Alkhudhiri A, Darwish N, Hilal N. Membrane distillation: A comprehensive review. Desalination 2012;287:2–18. https://doi.org/10.1016/j.desal.2011.08.027.

[9] Choi Y, Naidu G, Nghiem LD, Lee S, Vigneswaran S. Membrane distillation crystallization for brine mining and zero liquid discharge: Opportunities, challenges, and recent progress. Environ Sci Water Res Technol 2019;5:1202–21. https://doi.org/10.1039/c9ew00157c.

[10] Bogler A, Lin S, Bar-zeev E. Biofouling of membrane distillation, forward osmosis and pressure retarded osmosis: Principles, impacts and future directions. J Memb Sci 2017;542:378–98. https://doi.org/10.1016/j.memsci.2017.08.001.

[11] Tan HF, Tan WL, Hamzah N, Ng MHK, Ooi BS, Leo CP. Membrane distillation crystallization using PVDF membrane incorporated with TiO2 nanoparticles and nanocellulose, Water Sci. Technol. Water Supply 2020;20:1629–42. https://doi.org/10.2166/ws.2020.068.

[12] Nthunya LN, Bopape MF, Mahlangu OT, Mamba BB, Van der Bruggen B, Quist-Jensen CA, Richards H. Fouling, performance and cost analysis of membrane-based water desalination technologies: A critical review. J Environ Manag 2022;301:113922. https://doi.org/10.1016/j.jenvman.2021.113922.

[13] Ruiz-Aguirre A, Andrés-Mañas JA, Zaragoza G. Evaluation of permeate quality in pilot scale membrane distillation systems. Membr (Basel) 2019;9:1–14. https://doi.org/10.3390/membranes9060069.

[14] Dow N, Gray S, Li J de, Zhang J, Ostarcevic E, Liubinas A, Atherton P, Roeszler G, Gibbs A, Duke M. Pilot trial of membrane distillation driven by low grade waste heat: Membrane fouling and energy assessment. Desalination 2016;391:30–42. https://doi.org/10.1016/j.desal.2016.01.023.

[15] Gizer G, Önal U, Ram M, Sahiner N. Biofouling and Mitigation Methods: A Review. Biointerface Res Appl Chem 2023;13:1–25. https://doi.org/10.33263/BRIAC132.185.

[16] Costa FCR, Ricci BC, Teodoro B, Koch K, Drewes JE, Amaral MCS. Biofouling in membrane distillation applications - a review. Desalination 2021;516:115241. https://doi.org/10.1016/j.desal.2021.115241.

[17] Guo Y, Liu C, Liu H, Zhang J, Li H, Zhang C. Contemporary antibiofouling modifications of reverse osmosis membranes: State-of-the-art insights on mechanisms and strategies. Chem Eng J 2022;429:132400. https://doi.org/10.1016/j.cej.2021.132400.

[18] Jeong S, Vollprecht R, Cho K, Leiknes TO, Vigneswaran S, Bae H, Lee S. Advanced organic and biological analysis of dual media filtration used as a pretreatment in a full-scale seawater desalination plant. Desalination 2016;385:83–92. https://doi.org/10.1016/j.desal.2016.02.017.

[19] Mpala TJ, Etale A, Richards H, Nthunya LN. Biofouling phenomena in membrane distillation: mechanisms and mitigation strategies. Environ Sci Adv 2022;2:39–54. https://doi.org/10.1039/d2va00161f.

[20] Qi L, Jiang T, Liang R, Qin W. Polymeric membrane ion-selective electrodes with anti-biofouling properties by surface modification of silver nanoparticles. Sens Actuators, B Chem 2021;328:129014. https://doi.org/10.1016/j.snb.2020.129014.

[21] Mpala TJ, Serepa-dlamini MH, Etale A, Richards H, Nthunya LN. Cellulose nanocrystal-mediated synthesis of silver nanoparticles via microwave assisted method for biofouling control in membrane distillation. Mater Today Commun 2023;34:105028. https://doi.org/10.1016/j.mtcomm.2022.105028.

[22] Xu Q, Jin L, Wang Y, Chen H, Qin M. Synthesis of silver nanoparticles using dialdehyde cellulose nanocrystal as a multi-functional agent and application to antibacterial paper. Cellulose 2019;26:1309–21. https://doi.org/10.1007/s10570-018-2118-3.

[23] Hanif Z, Khan ZA, Choi D, La M, Park SJ. One-pot synthesis of silver nanoparticle deposited cellulose nanocrystals with high colloidal stability for bacterial contaminated water purification. J Environ Chem Eng 2021;9:105535. https://doi.org/10.1016/j.jece.2021.105535.

[24] Hanif Z, Khan ZA, Shin D, Choi D, Park SJ. Facile Deposition of Silver Nanoparticles on Photonic Cellulose Nanocrystals Films: A Study on Solvent Stability and Post Antibacterial Activity. Macromol Mater Eng 2021;306:1–8. https://doi.org/10.1002/mame.202100289.

[25] Musino D, Rosset A, Lelong C, Luche S, Bergé V, Brochard G, Plumail M, Trouiller B, Auger A, Guiot A, Patouillard J, Desrousseaux S, Artous S, Rabilloud T, Boutry D, Capron I. CNC/AgNP hybrids as safer-by-design biocides in paints -. Environ Sci Nano 2021;8:3673–84. https://doi.org/10.1039/D1EN00407G.

[26] Makgabutlane B, Nthunya LN, Maubane-Nkadimeng MS, Mhlanga SD. Green synthesis of carbon nanotubes to address the water-energy-food nexus: A critical review. J Environ Chem Eng 2021;9:104736. https://doi.org/10.1016/j.jece.2020.104736.

[27] C. Gao, W. Deng, F. Pan, X. Feng, Y. Li, Superhydrophobic Electrospun PVDF Membranes with Silanization and Fluorosilanization Co-Functionalized CNTs for Improved Direct Contact Membrane Distillation, (2020) 35–43. https://doi.org/10.30919/es8d905.

[28] Karimi A, Khataee A, Vatanpour V, Safarpour M. The effect of different solvents on the morphology and performance of the ZIF-8 modified PVDF ultrafiltration membranes. Sep Purif Technol 2020;253:117548. https://doi.org/10.1016/j.seppur.2020.117548.

[29] Kebria MRS, Rahimpour A. Membrane Distillation: Basics, Advances and Applications. Adv. Membr. Technol. Bol. London: Intechopen; 2020. p. 1–21. https://doi.org/10.5772/intechopen.86952.

[30] Yang G, Zhang J, Peng M, Du E, Wang Y, Shan G, Ling L, Ding H, Gray S, Xie Z. A mini review on antiwetting studies in membrane distillation for textile wastewater treatment. Processes 2021;9:1–16. https://doi.org/10.3390/pr9020243.

[31] Burgess SA, Flint SH, Lindsay D, Cox MP, Biggs PJ. Insights into the Geobacillus stearothermophilus species based on phylogenomic principles. BMC Microbiol 2017;17:1–12. https://doi.org/10.1186/s12866-017-1047-x.

[32] Mpala TJ, Richards H, Etale A, Mahlangu OT, Nthunya LN. Carbon nanotubes and silver nanoparticles modification of PVDF membranes for improved seawater desalination in direct contact membrane distillation. Front Membr Sci Technol 2023;2:1–11. https://doi.org/10.3389/frmst.2023.1165678.

[33] Mahlangu OT, Nthunya LN, Motsa MM, Morifi E, Richards H, Mamba BB. Fouling of high pressure-driven NF and RO membranes in desalination processes: Mechanisms and implications on salt rejection. Chem Eng Res Des 2023;199:268–95. https://doi.org/10.1016/j.cherd.2023.09.037.

[34] Mahlangu TO, Thwala JM, Mamba BB, D'Haese A, Verliefde ARD. Factors governing combined fouling by organic and colloidal foulants in cross-flow nanofiltration. J Memb Sci 2015;491:53–62. https://doi.org/10.1016/j.memsci.2015.03.021.

[35] Motsa MM, Mamba BB, Verliefde ARD. Forward osmosis membrane performance during simulated wastewater reclamation: Fouling mechanisms and fouling layer properties. J Water Process Eng 2018;23:109–18. https://doi.org/10.1016/j.jwpe.2018.03.007.

[36] Khumalo N, Nthunya L, Derese S, Motsa M, Verliefde A, Kuvarega A, Mamba BB, Mhlanga S, Dlamini DS. Water recovery from hydrolysed human urine samples via direct contact membrane distillation using PVDF/PTFE membrane. Sep Purif Technol 2019;211:610–7. https://doi.org/10.1016/j.seppur.2018.10.035.

[37] Janczuk B, Wojcik W, Zdziennicka A. Determination of the components of the surface tension of some liquids from interfacial liquid-liquid tension measurements. J Colloid Interface Sci 1993;157:384–93.

[38] Yu HY, Qin ZY, Sun B, Yan CF, Yao JM. One-pot green fabrication and antibacterial activity of thermally stable corn-like CNC/Ag nanocomposites. J Nanopart Res 2014;16:1–12. https://doi.org/10.1007/s11051-013-2202-4.

[39] Jatoi AW, Ogasawara H, Kim IS, Ni QQ. Dopa-based facile procedure to synthesize AgNP/cellulose nanofiber composite for antibacterial applications. Appl Nanosci 2019;9:1661–70. https://doi.org/10.1007/s13204-019-00952-3.

[40] Toro RG, Adel AM, de Caro T, Federici F, Cerri L, Bolli E, Mezzi A, Barbalinardo M, Gentili D, Cavallini M, Al-Shemy MT, Montanari R, Caschera D. Evaluation of long–lasting antibacterial properties and cytotoxic behavior of functionalized silver-nanocellulose composite. Mater (Basel) 2021;14. https://doi.org/10.3390/ma14154198.

[41] Badawy AA, Ghanem AF, Yassin MA, Youssef AM, Abdel Rehim MH. Utilization and characterization of cellulose nanocrystals decorated with silver and zinc oxide nanoparticles for removal of lead ion from wastewater. Environ Nanotechnol, Monit Manag 2021;16:100501. https://doi.org/10.1016/j.enmm.2021.100501.

[42] Zhao L, Qu X, Zhang M, Lin H, Zhou X, Liao B, Mei R, Hong H. Influences of acid – base property of membrane on interfacial interactions related with membrane fouling in a membrane bioreactor based on thermodynamic assessment. Bioresour Technol 2016;214:355–62. https://doi.org/10.1016/j.biortech.2016.04.080.

[43] Jiang S, Li Y, Ladewig BP. A review of reverse osmosis membrane fouling and control strategies. Sci Total Environ 2017;595:567–83. https://doi.org/10.1016/j.scitotenv.2017.03.235.

[44] Bogler A, Bar-Zeev E. Membrane Distillation Biofouling: Impact of Feedwater Temperature on Biofilm Characteristics and Membrane Performance. Environ Sci Technol 2018;52:10019–29. https://doi.org/10.1021/acs.est.8b02744.

[45] Elcik H, Alpatova A, Gonzalez-Gil G, Blankert B, Farhat N, Amin NA, Vrouwenvelder JS, Ghaffour N. Elucidating biofouling over thermal and spatial gradients in seawater membrane distillation in hot climatic conditions. Water Res 2022;223:118983. https://doi.org/10.1016/j.watres.2022.118983.

[46] M. Rezaei, Wetting Prevention in Membrane Distillation, (2017).

[47] Al-Araji D, Al-Ani F, Alsalhy Q. The permeation and Separation Characteristics of Polymeric Membranes Incorporated with Nanoparticles for Dye Removal and Interaction Mechanisms between Polymer and Nanoparticles: A Mini Review. Eng Technol J 2022;40:1399–411. https://doi.org/10.30684/etj.2022.132572.1129.

[48] Mahlangu OT, Motsa MM, Richards H, Mamba BB, George MJ, Nthunya LN. The impact of nanoparticle leach on sustainable performance of the membranes – A critical review. Environ Nanotechnol Monit Manag 2024;22:100984. https://doi.org/10.1016/j.enmm.2024.100984.

[49] Amin NA, Elcik H, Alpatova A, Gonzalez-Gil G, Blankert B, Farhat N, Vrouwenvelder JS, Ghaffour N. Selected physical and chemical cleanings remove biofilm in seawater membrane distillation without causing pore wetting. Npj Clean Water 2023;6:1–12. https://doi.org/10.1038/s41545-023-00278-2.

[50] Zodrow KR, Bar-Zeev E, Giannetto MJ, Elimelech M. Biofouling and Microbial Communities in Membrane Distillation and Reverse Osmosis. Environ Sci Technol 2014;48:13155–64. https://doi.org/10.1021/es503051t.

[51] Liu C, Zhu L, Chen L. Biofouling phenomenon of direct contact membrane distillation (DCMD) under two typical operating modes: Open-loop mode and closed-loop mode. J Memb Sci 2020;601:11792. https://doi.org/10.1016/j.memsci.2020.117952.

[52] Nthunya LN, Gutierrez L, Khumalo N, Derese S, Mamba BB, Verliefde AR, Mhlanga SD. Superhydrophobic PVDF nanofibre membranes coated with an organic fouling resistant hydrophilic active layer for direct-contact membrane distillation. Colloids Surf A Physicochem Eng Asp 2019;575:363–72. https://doi.org/10.1016/j.colsurfa.2019.05.031.

[53] Zheng L, Zhang C, Kang S, Li C, Hou D, Wu S, Wang J, Wei Y. Insight into the microbial distribution and succession and biofouling mechanism in membrane distillation for desulfurization wastewater treatment. Chem Eng J 2022;428:131097. https://doi.org/10.1016/j.cej.2021.131097.

[54] Yu Z, Wang W, Dhital R, Kong F, Lin M, Mustapha A. Antimicrobial effect and toxicity of cellulose nanofibril / silver nanoparticle nanocomposites prepared by an ultraviolet irradiation method. Colloids Surf B Biointerfaces 2019;180:212–20. https://doi.org/10.1016/j.colsurfb.2019.04.054.

[55] Xu C, Chen W, Gao H, Xie X, Chen Y. Cellulose nanocrystal/silver (CNC/Ag) thin-film nanocomposite nanofiltration membranes with multifunctional properties. Environ Sci Nano 2020;7:803–16. https://doi.org/10.1039/c9en01367a.

[56] Xuan L, Tian LJ, Tian T, Wang XM, Yang DH, Yu HQ. In situ synthesizing silver nanoparticels by bio-derived gallic acid to enhance antimicrobial performance of PVDF membrane. Sep Purif Technol 2020;251:117381. https://doi.org/10.1016/j.seppur.2020.117381.
[57] Barrios AC, Carrillo D, Waag TR, Rice D, Bi Y, Islam R, Perreault F. Prolonging the antibacterial activity of nanosilver-coated membranes through partial sulfidation. Environ Sci Nano 2020;7:2607–17. https://doi.org/10.1039/d0en00300j.
[58] Ma Z, Liu J, Shen G, Zheng X, Pei Y, Tang K. In-situ synthesis and immobilization of silver nanoparticles on microfibrillated cellulose for long-term antibacterial applications. Cellulose 2021;28:6287–303. https://doi.org/10.1007/s10570-021-03941-4.
[59] Susanti D, Haris MS, Taher M, Khotib J. Natural Products-Based Metallic Nanoparticles as Antimicrobial Agents. Front Pharmacol 2022;13:1–14. https://doi.org/10.3389/fphar.2022.895616.
[60] Choudhury MR, Anwar N, Jassby D, Rahaman MS. Fouling and wetting in the membrane distillation driven wastewater reclamation process – A review. Adv Colloid Interface Sci 2019;269:370–99. https://doi.org/10.1016/j.cis.2019.04.008.
[61] Medeiros KAR, Rangel EQ, Sant'Anna AR, Louzada DR, Barbosa CRH, D'Almeida JRM. Evaluation of the electromechanical behavior of polyvinylidene fluoride used as a component of risers in the offshore oil industry. Oil Gas Sci Technol 2018;73:1–7. https://doi.org/10.2516/ogst/2018058.
[62] Ryu SR, Noda I, Jung YM. What is the origin of positional fluctuation of spectral features: True frequency shift or relative intensity changes of two overlapped bands? Appl Spectrosc 2010;64:1017–21. https://doi.org/10.1366/000370210792434396.
[63] Nguyen PT, Nguyen TT, Bui DC, Hong PT, Hoang QK, Nguyen HT. Exopolysaccharide production by lactic acid bacteria: The manipulation of environmental stresses for industrial applications. AIMS Microbiol 2020;6:451–69. https://doi.org/10.3934/MICROBIOL.2020027.